

Low Energy Neutrino Cross Sections: Comparison of Various Monte Carlo Predictions to Experimental Data

G.P. Zeller^a

^aColumbia University, Department of Physics, New York, NY 10027

Charged current (CC) and neutral current (NC) low energy neutrino cross section predictions from a variety of Monte Carlo generators in present use are compared against existing experimental data. Comparisons are made to experimental data on quasi-elastic, resonant and coherent single pion production, multiple pion production, single kaon production, and total inclusive cross sections, and are restricted to the case of ν_μ scattering off free nucleons.

1. Introduction

Present atmospheric and accelerator based neutrino oscillation experiments operate at low neutrino energies ($E_\nu \sim 1$ GeV) to access the relevant regions of oscillation parameter space. As such, they require precise knowledge of the cross sections for neutrino-nucleon interactions in the sub-to-few GeV range. At these energies, neutrino interactions are predominantly quasi-elastic (QE) or single pion production processes (Figure 1), which historically have not been as well studied as deep inelastic scattering (DIS) reactions which dominate at higher energies.

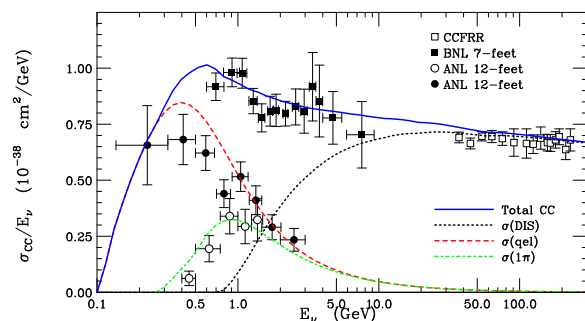


Figure 1. Charged current neutrino cross sections as a function of energy (in GeV). Shown are the contributions from quasi-elastic (dashed), single pion (dot-dash) and deep inelastic scattering (dotted) processes. Figure from Reference [1].

Data on quasi-elastic scattering and single pion

production come mainly from bubble chamber, spark chamber, and emulsion experiments that ran decades ago. Despite relatively poor statistics and large neutrino flux uncertainties, they provide an important and necessary constraint on Monte Carlo models in present use. Recent neutrino experiments employ a variety of Monte Carlo generators to model low energy neutrino interaction cross sections. Many share common theoretical inputs such as Llewellyn Smith free nucleon QE cross sections [7], Rein and Sehgal-based resonance production [16], along with standard DIS formulas and parton distribution functions. Yet the generators can differ substantially in how they implement Fermi gas models, combine resonance and DIS regions, and treat nuclear and final state effects [1]. This work is an attempt to compare several Monte Carlo generators to the existing body of low energy neutrino cross section data. In particular, three simulations are considered: v2 NUANCE [2], NEUGEN [3], and NUX [4]. For the purpose of comparison, the Monte Carlo cross section predictions in each case have been generated under the same set of parameter assumptions [5], namely: $m_A = 1.032$ GeV, $m_V = 0.84$ GeV, $g_A = -1.25$, and $\sin^2 \theta_W = 0.233$ where applicable. While only free nucleon cross section comparisons are presented here, detailed comparisons of generated Monte Carlo event kinematics are provided in [6].

2. Quasi-Elastic Scattering

At low energies, CC neutrino hadron interactions are predominantly quasi-elastic:

$$\nu_\mu n \rightarrow \mu^- p$$

In predicting the cross section for quasi-elastic scattering off free nucleons, most Monte Carlos commonly employ the Llewellyn Smith formalism [7] in which the QE differential cross section takes the form:

$$\frac{d\sigma}{dQ^2} = \frac{G_F^2 M^2}{8\pi E_\nu} \left[A \mp \frac{(s-u)}{M^2} B + \frac{(s-u)^2}{M^4} C \right] \quad (1)$$

where (+)− refers to (anti)neutrino scattering, G_F is the Fermi coupling constant, Q^2 is the squared four-momentum transfer ($Q^2 = -q^2 > 0$), M is the nucleon mass, E_ν is the incident neutrino energy, and $(s-u) = 4ME_\nu - Q^2 - m^2$. The factors A , B , and C are functions of the two vector form factors F_1 and F_2 , the axial vector form factor F_A , and the pseudoscalar form factor F_P :

$$\begin{aligned} A = & \frac{(m^2 + Q^2)}{M^2} \left[(1 + \tau) F_A^2 - (1 - \tau) F_1^2 \right. \\ & + \tau (1 - \tau) F_2^2 + 4\tau F_1 F_2 \\ & \left. - \frac{m^2}{4M^2} ((F_1 + F_2)^2 + (F_A + 2F_P)^2 \right. \\ & \left. - \left(\frac{Q^2}{M^2} + 4 \right) F_P^2 \right) \right] \quad (2) \end{aligned}$$

$$B = \frac{Q^2}{M^2} F_A (F_1 + F_2) \quad (3)$$

$$C = \frac{1}{4} (F_A^2 + F_1^2 + \tau F_2^2) \quad (4)$$

where $\tau = Q^2/4M^2$ and m is the muon mass. Monte Carlos commonly assume a dipole form for the factors F_1 , F_2 , F_A , and F_P :

$$F_1(Q^2) = \frac{1 + \tau (1 + \mu_p - \mu_n)}{(1 + \tau) \left(1 + \frac{Q^2}{m_V^2} \right)^2} \quad (5)$$

$$F_2(Q^2) = \frac{(\mu_p - \mu_n)}{(1 + \tau) \left(1 + \frac{Q^2}{m_V^2} \right)^2} \quad (6)$$

$$F_A(Q^2) = \frac{g_A}{\left(1 + \frac{Q^2}{m_A^2} \right)^2}; \quad g_A = -1.25 \quad (7)$$

$$F_P(Q^2) = \frac{2M^2}{m_\pi^2 + Q^2} F_A(Q^2) \quad (8)$$

where m_π is the pion mass, $\mu_p = 1.793 \mu_N$ and $\mu_n = -1.913 \mu_N$ are the proton and neutron anomalous magnetic moments, respectively, and the parameters m_V , m_A , and g_A are empirical inputs [5]. Departures from this dipole approximation which better fit electron scattering data have recently been explored and have few-% effects on the shape of the predicted cross section [8].

Over the years, quasi-elastic processes have been studied extensively in bubble chamber experiments at ANL, BNL, CERN, FNAL, and Serpukhov. The bulk of this data came from light targets and had limited precision due to large neutrino flux uncertainties. Figure 2 compares the various Monte Carlo predictions to this collection of QE cross section data. It is no surprise that given the same underlying model and input parameters, the various Monte Carlo predictions agree up to their numerical precision; however, note that there is a large spread in the available experimental data.

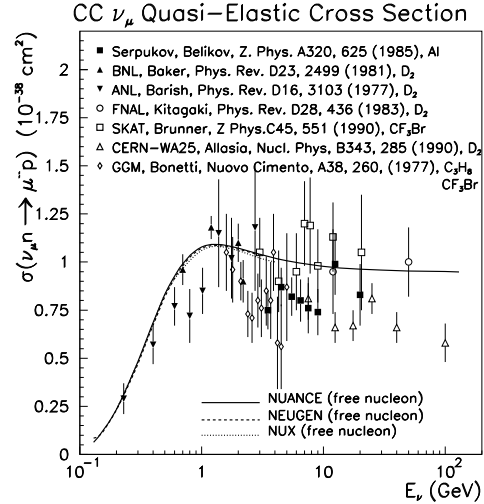


Figure 2. QE data compared to various Monte Carlo calculations assuming a dipole form for the vector and axial vector form factors with $m_V = 0.84$ GeV, $m_A = 1.032$ GeV, and $g_A = -1.25$.

3. NC Elastic Scattering

Neutrinos can also elastically scatter from both protons and neutrons in the target material:

$$\nu_\mu p \rightarrow \nu_\mu p$$

$$\nu_\mu n \rightarrow \nu_\mu n$$

Equations 1-4 still apply in describing the neutral current elastic scattering cross section with the exception that in this case the form factors include additional coupling factors and a contribution from strange quarks:

$$\begin{aligned} F_1(Q^2) &= \left(\frac{1}{2} - \sin^2 \theta_W \right) \left[\frac{\tau_3(1 + \tau(1 + \mu_p - \mu_n))}{(1 + \tau)(1 + Q^2/m_V^2)^2} \right] \\ &\quad - \sin^2 \theta_W \left[\frac{1 + \tau(1 + \mu_p + \mu_n)}{(1 + \tau)(1 + Q^2/m_V^2)^2} \right] - \frac{F_1^s(Q^2)}{2} \\ F_2(Q^2) &= \left(\frac{1}{2} - \sin^2 \theta_W \right) \frac{\tau_3(\mu_p - \mu_n)}{(1 + \tau) \left(1 + \frac{Q^2}{m_V^2} \right)^2} \\ &\quad - \sin^2 \theta_W \frac{\mu_p + \mu_n}{(1 + \tau) \left(1 + \frac{Q^2}{m_V^2} \right)^2} - \frac{F_2^s(Q^2)}{2} \\ F_A(Q^2) &= \frac{g_A \tau_3}{2 \left(1 + \frac{Q^2}{m_A^2} \right)^2} + \frac{F_A^s(Q^2)}{2} \end{aligned}$$

where $g_A = -1.25$ and $\tau_3 = +1(-1)$ for proton (neutron) scattering. $F_{1,2}^s(Q^2)$ are the strange vector form factors; the strange axial vector form factor is commonly denoted as:

$$F_A^s(Q^2) = \frac{\Delta s}{\left(1 + \frac{Q^2}{m_A^2} \right)^2} \quad (9)$$

where Δs is the strange quark contribution to the nucleon spin.

Experiments typically publish NC elastic cross sections with respect to the CC QE cross section to minimize systematics. Table 1 lists a collection of experimental measurements of the NC/CC ratio, $(\nu_\mu p \rightarrow \nu_\mu p)/(\nu_\mu n \rightarrow \mu^- p)$. Figure 3 shows a comparison between the Monte Carlo calculations and the most precise measurement of

this ratio from BNL E734 [9]. While the BNL E734 result is quoted over a particular Q^2 range (Table 1), no Q^2 restrictions have been placed on the Monte Carlo predictions. Also note that NEUGEN is $\sim 20\%$ larger than the other predictions. This is simply because NEUGEN assumes $\Delta s = -0.15$, which enters the differential cross section as $(\Delta s)^2$, whereas the other models assume $\Delta s = 0$ by default [10].

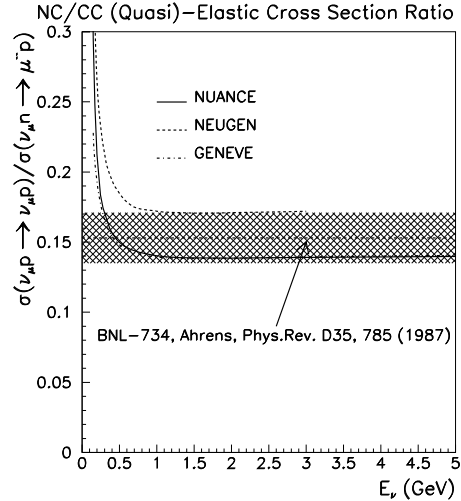


Figure 3. Most precise measurement of the NC/CC ratio, $(\nu_\mu p \rightarrow \nu_\mu p)/(\nu_\mu n \rightarrow \mu^- p)$, compared to predictions from NUANCE, NEUGEN, and another neutrino generator, GENEVE [15].

Experiment	Target	Result	$Q^2(\text{GeV}^2)$
BNL E734 [9]	CH_2	0.153 ± 0.018	$0.5 \rightarrow 1.0$
BNL CIB [11]	Al	0.11 ± 0.03	$0.3 \rightarrow 0.9$
Aachen [12]	Al	0.10 ± 0.03	$0.2 \rightarrow 1.0$
BNL E613 [13]	CH_2	0.11 ± 0.02	$0.4 \rightarrow 0.9$
Gargamelle [14]	CF_3Br	0.12 ± 0.06	$0.3 \rightarrow 1.0$

Table 1

Several measurements of the ratio, $(\nu_\mu p \rightarrow \nu_\mu p)/(\nu_\mu n \rightarrow \mu^- p)$. Also indicated is the Q^2 interval over which the ratio was measured.

4. CC and NC Single Pion Production

The dominant means of single pion production in low energy neutrino interactions arises through the excitation of a baryon resonance (N^*) which then decays to a nucleon-pion final state:

$$\begin{aligned}\nu_\mu N &\rightarrow l^- N^* \\ N^* &\rightarrow \pi N'\end{aligned}$$

where $N, N' = n, p$. There are seven possible resonant single pion reaction channels, three charged current:

$$\begin{aligned}\nu_\mu p &\rightarrow \mu^- p \pi^+ \\ \nu_\mu n &\rightarrow \mu^- p \pi^0 \\ \nu_\mu n &\rightarrow \mu^- n \pi^+\end{aligned}$$

and four neutral current:

$$\begin{aligned}\nu_\mu p &\rightarrow \nu_\mu p \pi^0 \\ \nu_\mu p &\rightarrow \nu_\mu n \pi^+ \\ \nu_\mu n &\rightarrow \nu_\mu n \pi^0 \\ \nu_\mu n &\rightarrow \nu_\mu p \pi^-\end{aligned}$$

Traditionally, Monte Carlo base their theoretical calculations of resonant pion production on the Rein and Sehgal model [16]. While the $\Delta(1232)$ is the dominant resonance at these energies, both the NUANCE and NEUGEN generators include additional higher mass resonant states. In contrast, the NUX model does not yet contain explicit resonance production, and is thus why the NUX predictions exhibit less agreement with the data. Such models are commonly tuned to reproduce single pion data, but remain poorly constrained because of the limited availability and large uncertainties in this data. With a few exceptions, most of the experimental measurements come from deuterium or hydrogen target bubble chamber experiments. Figures 4-6 compare the Monte Carlo predictions to available CC single pion data. The NUANCE and NEUGEN predictions include both resonant and nonresonant contributions and assume no invariant mass restrictions. Some caution is warranted in drawing conclusions from these plots as some of the higher energy data includes a $W < 2.0$ GeV invariant mass cut. The data sets with W cuts are indicated in each caption.

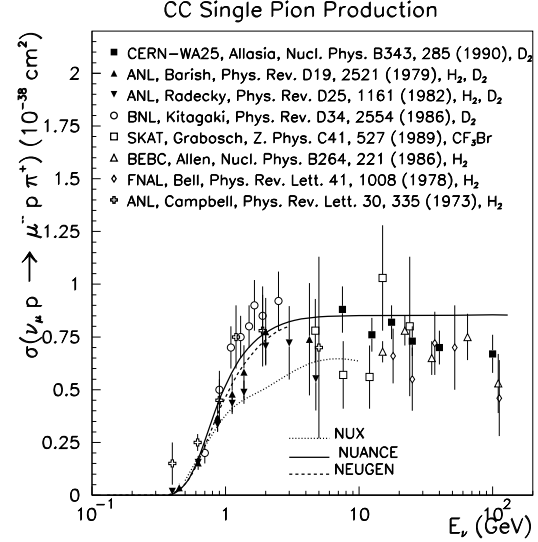


Figure 4. Measurements of the CC 1π cross section $\sigma(\nu_\mu p \rightarrow \mu^- p \pi^+)$. The Monte Carlo assume $m_A = 1.032$ GeV and $m_V = 0.84$ GeV. The data do not include an invariant mass cut with the exception of the CERN-WA25, SKAT, BEBC, and FNAL measurements which are reported for $W < 2.0$ GeV.

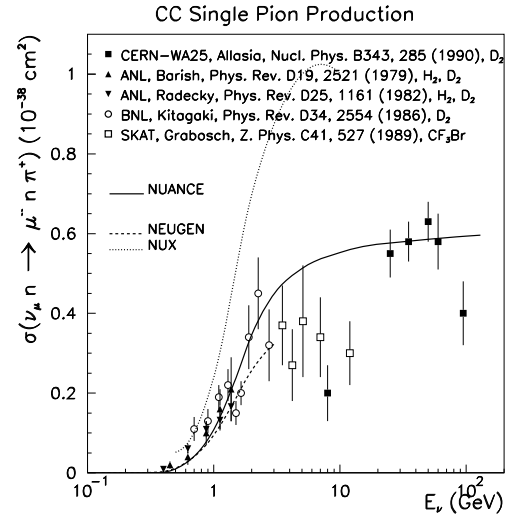


Figure 5. Measurements of the CC 1π cross section $\sigma(\nu_\mu n \rightarrow \mu^- n \pi^+)$. The data do not include an invariant mass cut with the exception of the CERN-WA25 and SKAT measurements which are reported for $W < 2.0$ GeV.

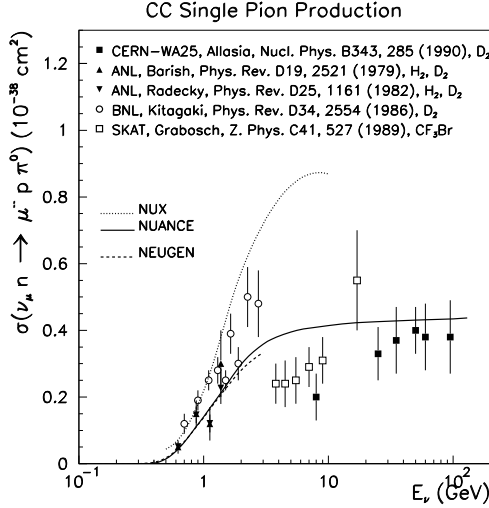


Figure 6. CC 1π cross section $\sigma(\nu_\mu n \rightarrow \mu^- p \pi^0)$. Same Monte Carlo and data criteria as in Figure 5. Note: the CERN-WA25 data on this channel as reported in the Durham reaction database is actually the sum of their measured $\nu_\mu n \rightarrow \mu^- p \pi^0$ and $\nu_\mu n \rightarrow \mu^- n \pi^+$ cross sections [17].

The data on NC single pion cross sections is even more limited. Almost all of this data exists in the form of NC/CC ratios. Table 2 summarizes the various measurements, all of which were conducted using bubble chambers with the exception of BNL and CERN PS which both utilized spark chambers. In some instances, the experimental data can differ by as much as factors of two or three. Also listed are the predictions from NUANCE. In all cases, the NUANCE Monte Carlo agrees with at least one measurement.

Furthermore, data on **absolute** inclusive NC single pion cross sections is extremely sparse. While the ANL 12 ft deuterium bubble chamber experiment [25], reported a cross section for the NC $1\pi^-$ channel, $\nu_\mu n \rightarrow \nu_\mu p \pi^-$, the only measurements of the remaining NC 1π cross sections come from a recent reanalysis of Gargamelle propane-freon bubble chamber data [20]. Figures 7-10 compare these measurements to resonant + nonresonant predictions from NUANCE and NEUGEN. Both the data and Monte Carlo in all cases have been corrected to free nucleon cross sections.

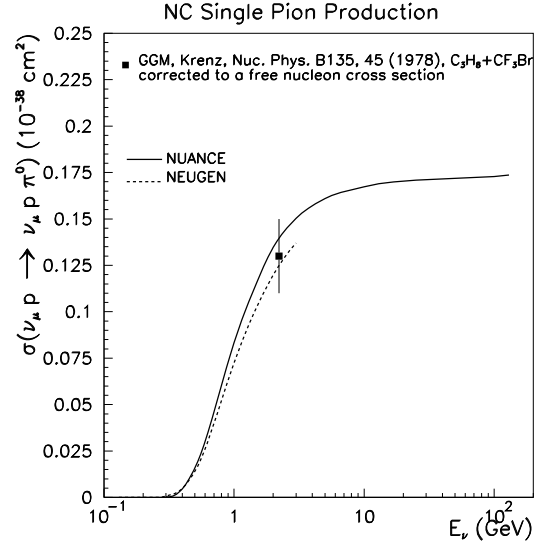


Figure 7. NC 1π cross section $\sigma(\nu_\mu p \rightarrow \nu_\mu p \pi^0)$. Shown are the free nucleon cross section predictions from NUANCE and NEUGEN with $m_A = 1.032$ GeV, $m_V = 0.84$ GeV, and $\sin^2 \theta_W = 0.233$.

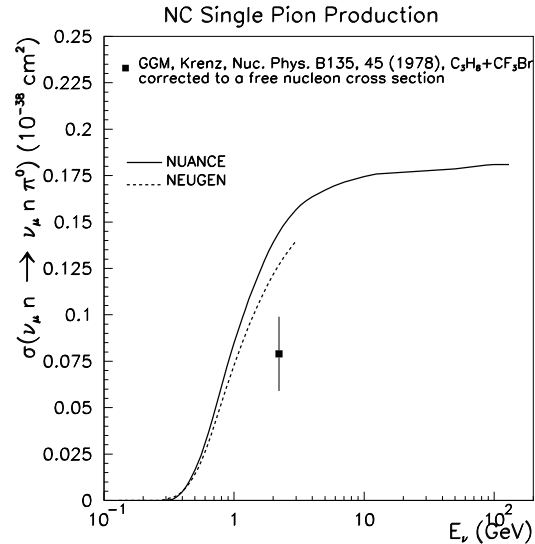


Figure 8. NC 1π cross section $\sigma(\nu_\mu n \rightarrow \nu_\mu n \pi^0)$. Same Monte Carlo settings as in Figure 7.

Source	Target	NC/CC Ratio	Value	Ref
ANL	H_2	$\sigma(\nu_\mu p \rightarrow \nu_\mu p \pi^0)/\sigma(\nu_\mu p \rightarrow \mu^- p \pi^+)$	$0.51 \pm 0.25^*$	[18]
ANL	H_2	$\sigma(\nu_\mu p \rightarrow \nu_\mu p \pi^0)/\sigma(\nu_\mu p \rightarrow \mu^- p \pi^+)$	$0.09 \pm 0.05^*$	[19]
NUANCE	free nucleon	$\sigma(\nu_\mu p \rightarrow \nu_\mu p \pi^0)/\sigma(\nu_\mu p \rightarrow \mu^- p \pi^+)$	0.20	[2]
ANL	H_2	$\sigma(\nu_\mu p \rightarrow \nu_\mu n \pi^+)/\sigma(\nu_\mu p \rightarrow \mu^- p \pi^+)$	0.17 ± 0.08	[18]
ANL	H_2	$\sigma(\nu_\mu p \rightarrow \nu_\mu n \pi^+)/\sigma(\nu_\mu p \rightarrow \mu^- p \pi^+)$	0.12 ± 0.04	[19]
NUANCE	free nucleon	$\sigma(\nu_\mu p \rightarrow \nu_\mu n \pi^+)/\sigma(\nu_\mu p \rightarrow \mu^- p \pi^+)$	0.17	[2]
ANL	D_2	$\sigma(\nu_\mu n \rightarrow \nu_\mu p \pi^-)/\sigma(\nu_\mu n \rightarrow \mu^- n \pi^+)$	0.38 ± 0.11	[21]
NUANCE	free nucleon	$\sigma(\nu_\mu n \rightarrow \nu_\mu p \pi^-)/\sigma(\nu_\mu n \rightarrow \mu^- n \pi^+)$	0.27	[2]
Gargamelle	C_3H_8 CF_3Br	$\Sigma_{N=n,p} \sigma(\nu_\mu N \rightarrow \nu_\mu N \pi^0)/2\sigma(\nu_\mu n \rightarrow \mu^- p \pi^0)$	0.45 ± 0.08	[22]
CERN PS	Al	$\Sigma_{N=n,p} \sigma(\nu_\mu N \rightarrow \nu_\mu N \pi^0)/2\sigma(\nu_\mu n \rightarrow \mu^- p \pi^0)$	0.40 ± 0.06	[21]
BNL	Al	$\Sigma_{N=n,p} \sigma(\nu_\mu N \rightarrow \nu_\mu N \pi^0)/2\sigma(\nu_\mu n \rightarrow \mu^- p \pi^0)$	$0.17 \pm 0.04^{**}$	[23]
BNL	Al	$\Sigma_{N=n,p} \sigma(\nu_\mu N \rightarrow \nu_\mu N \pi^0)/2\sigma(\nu_\mu n \rightarrow \mu^- p \pi^0)$	$0.248 \pm 0.085^{**}$	[24]
NUANCE	free nucleon	$\Sigma_{N=n,p} \sigma(\nu_\mu N \rightarrow \nu_\mu N \pi^0)/2\sigma(\nu_\mu n \rightarrow \mu^- p \pi^0)$	0.41	[2]
ANL	D_2	$\sigma(\nu_\mu n \rightarrow \nu_\mu p \pi^-)/\sigma(\nu_\mu p \rightarrow \mu^- p \pi^+)$	0.11 ± 0.022	[19]
NUANCE	free nucleon	$\sigma(\nu_\mu n \rightarrow \nu_\mu p \pi^-)/\sigma(\nu_\mu p \rightarrow \mu^- p \pi^+)$	0.19	[2]

Table 2

Measurements of NC/CC single pion cross section ratios. The Gargamelle data has been corrected to a free nucleon ratio [22]. Also quoted are the free nucleons cross section predictions from NUANCE assuming $m_A = 1.032$ GeV, $m_V = 0.84$, and $\sin^2 \theta_W = 0.2319$ in each case. * In their later paper [19], Derrick *et al.* remark that while this result is 1.6σ smaller than their previous result [18], the neutron background in this case was better understood. ** The BNL NC π^0 data was later reanalyzed after properly taking into account multi- π backgrounds and found to have a larger fractional cross section [24].

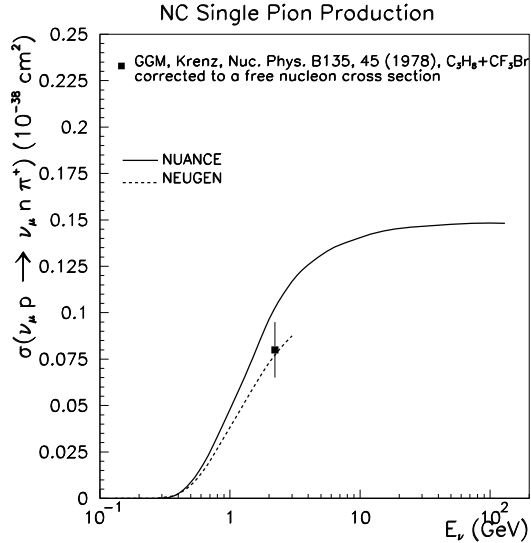


Figure 9. NC 1π cross section $\sigma(\nu_\mu p \rightarrow \nu_\mu n \pi^+)$. Same Monte Carlo settings as in Figure 7.

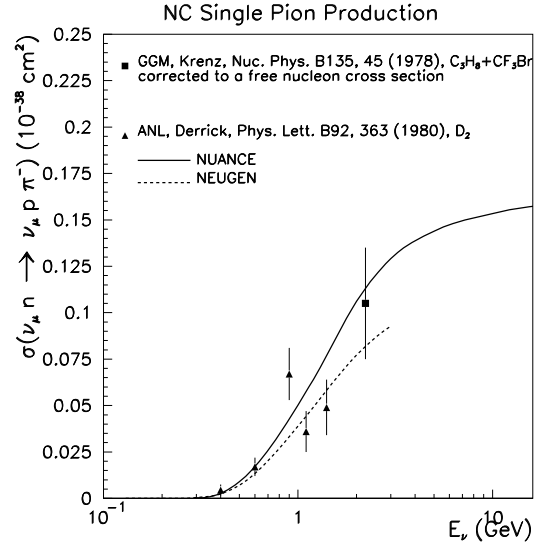


Figure 10. NC cross section $\sigma(\nu_\mu n \rightarrow \nu_\mu p \pi^-)$. Same Monte Carlo settings as in Figure 7.

5. Single Pion Kinematic Comparisons

So far these comparisons have been restricted to the case of free nucleon cross sections; however, comparisons can also be made to measured kinematic distributions. Such evaluations were originally performed in testing NEUGEN generator performance and presented at NuInt01 [3]. The study is repeated here after including similar NUANCE calculations. Figures 11-12 display invariant mass and Q^2 distributions for the three CC single pion channels as measured in the BNL 7 foot deuterium bubble chamber [26]. Both the NUANCE and NEUGEN Monte Carlo predictions were generated assuming the BNL flux and deuterium target. The Monte Carlo normalization in all plots is determined by the peak of the $\nu_\mu p \rightarrow \mu^- p \pi^+$ invariant mass distribution in the data. Both Monte Carlo models yield comparable agreement with the experimental data.

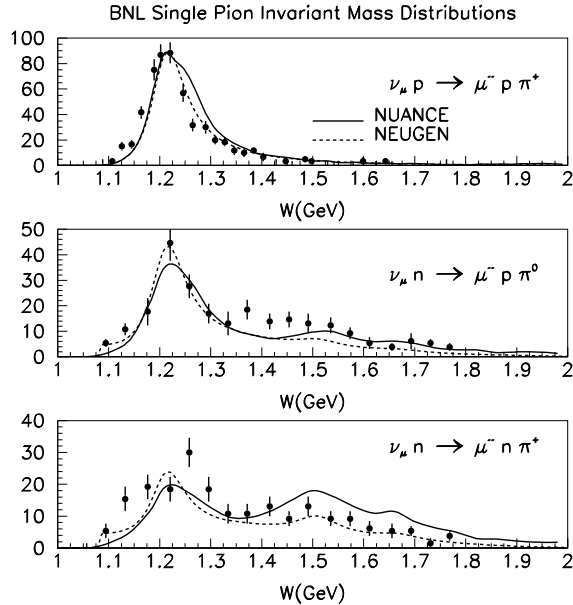


Figure 11. Invariant mass distributions (W) for CC single pion production channels as measured in Reference [26]. Note the clear $\Delta(1232)$ peak.

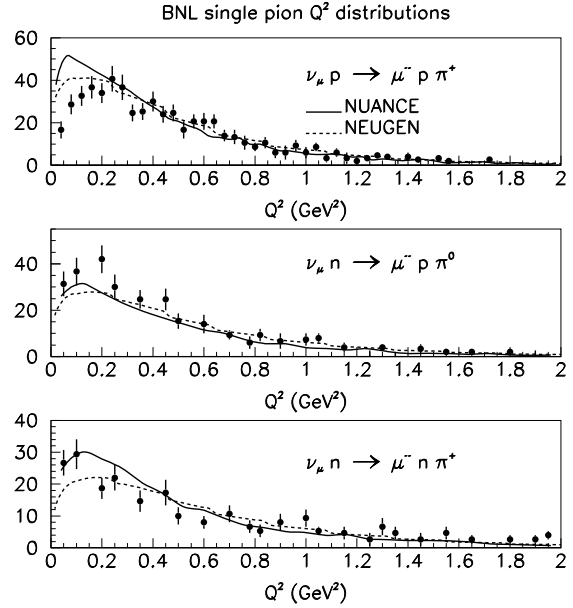


Figure 12. Four-momentum transfer (Q^2) distributions for CC 1π channels as measured in [26].

6. Coherent Pion Production

In addition to resonance production, neutrinos can also coherently produce single pion final states. In this case, the neutrino coherently scatters from the entire nucleus, transferring negligible energy to the target (A). The result is a distinctly forward-scattered single pion. Both NC and CC coherent pion production processes are possible:

$$\begin{aligned}\nu_\mu A &\rightarrow \nu_\mu A \pi^0 \\ \nu_\mu A &\rightarrow \mu^- A \pi^+\end{aligned}$$

The cross sections for such processes are predicted to be small, but have been measured in a variety of neutrino experiments. A comprehensive review of the experimental data is provided in Reference [27]. Figures 13 and 14 show a comparison of this data to the NUANCE and NEUGEN predictions. Both NC and CC data are displayed on the same plot after rescaling the NC data, assuming $\sigma_{NC}^{coh} = 1/2 \sigma_{CC}^{coh}$ [28]. In addition, data from various targets are corrected to oxygen cross sections assuming $A^{1/3}$ scaling [28].

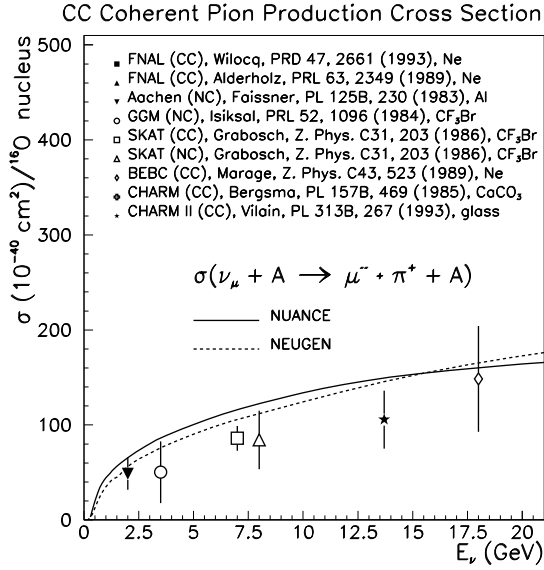


Figure 13. Coherent pion production data. In this comparison, NUANCE assumes $m_A = 1.032$ GeV while NEUGEN uses $m_A = 1.0$ GeV.

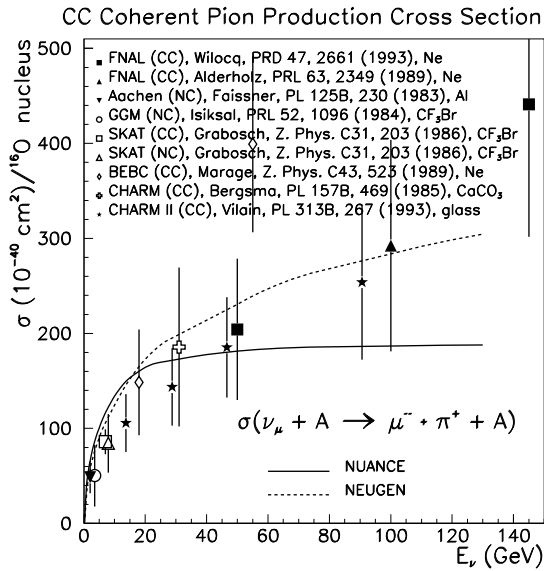


Figure 14. Same as Figure 13 except extended out to higher energies.

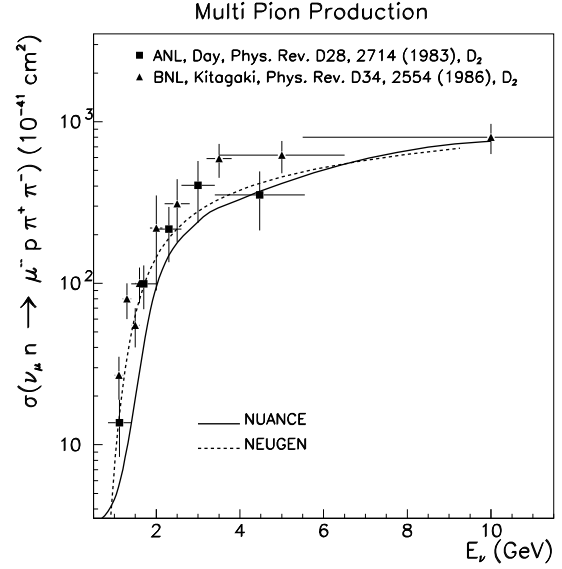


Figure 15. Cross section for $\nu_\mu n \rightarrow \mu^- p \pi^+ \pi^-$.

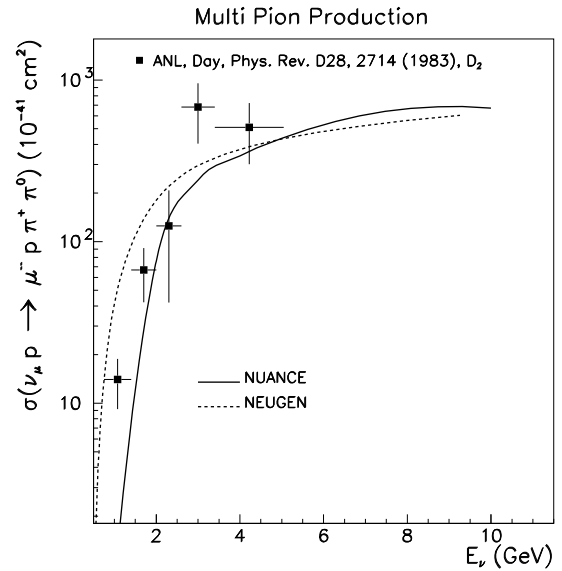


Figure 16. Cross section for $\nu_\mu p \rightarrow \mu^- p \pi^+ \pi^0$.

7. Multi-Pion Production

Because of the complexities involved in final state identification and isolation, data on multiple pion production is even less abundant and less precise than single pion production channels. Likewise, such channels exhibit the largest spread in the Monte Carlo estimates. Figures 15-17 compare available data on dipion production to NUANCE and NEUGEN. Because deep inelastic scattering is a large contribution to such cross sections, the NUANCE prediction is expected to improve with planned DIS model upgrades [29].

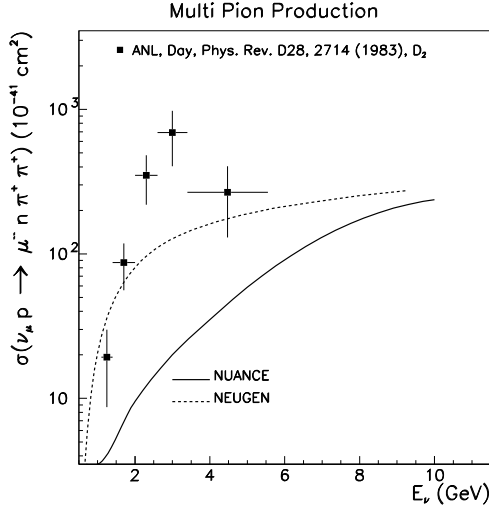


Figure 17. Cross section for $\nu_\mu p \rightarrow \mu^- n \pi^+ \pi^+$.

8. Single Kaon Production

Proton decay modes containing a final state kaon, $p \rightarrow \nu K^+$, have large branching ratios in many SUSY GUT models. Because there is a non-zero probability that an atmospheric neutrino interaction can mimic such a proton decay signature, estimating these background rates is an important component to such searches. The following lists some of the contributing strange production channels available at low energies:

CC :	NC :
$\nu_\mu n \rightarrow \mu^- K^+ \Lambda^0$	$\nu_\mu p \rightarrow \nu_\mu K^+ \Lambda^0$
$\nu_\mu p \rightarrow \mu^- K^+ p$	$\nu_\mu n \rightarrow \nu_\mu K^0 \Lambda^0$
$\nu_\mu n \rightarrow \mu^- K^0 p$	$\nu_\mu p \rightarrow \nu_\mu K^+ \Sigma^0$

$$\begin{aligned}
 \nu_\mu n &\rightarrow \mu^- K^+ n & \nu_\mu p &\rightarrow \nu_\mu K^0 \Sigma^+ \\
 \nu_\mu p &\rightarrow \mu^- K^+ \Sigma^+ & \nu_\mu n &\rightarrow \nu_\mu K^0 \Sigma^0 \\
 \nu_\mu n &\rightarrow \mu^- K^+ \Sigma^0 & \nu_\mu n &\rightarrow \nu_\mu K^+ \Sigma^- \\
 \nu_\mu n &\rightarrow \mu^- K^0 \Sigma^+ & \nu_\mu n &\rightarrow \nu_\mu K^- \Sigma^+
 \end{aligned} \quad (10)$$

Typically, such reactions have smaller cross sections than their single pion counterparts due to the kaon mass and because the kaon channels are not enhanced by any dominant resonance (in contrast to $\Delta(1232)$ decays to single pion final states). There are few predictive theoretical models for single kaon production [30] and little experimental data. Most of the data comes from bubble chamber measurements where the strange particle decays could be explicitly identified. Figure 18 shows the only two experiments which have published cross sections on the dominant associated production channel, $\nu_\mu n \rightarrow \mu^- K^+ \Lambda^0$. Both bubble chamber measurements were made on a deuterium target and based on less than 30 events combined. To model kaon production, NUANCE and NEUGEN employ the same Rein and Sehgal-based framework [16] as used to model single pion production, including additional resonance decays other than $N^* \rightarrow \pi N$. Note that as plotted, neither Monte Carlo includes DIS contributions to this channel.

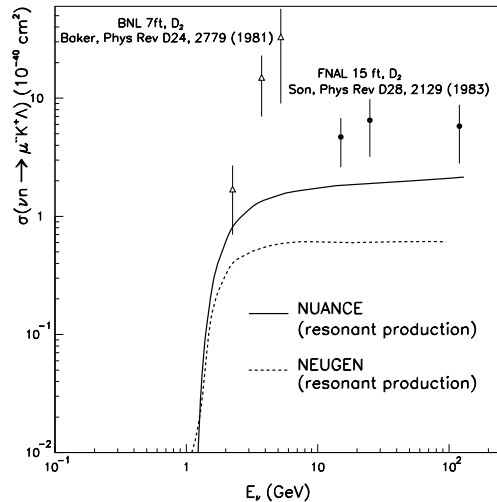


Figure 18. Measurements of the associated production cross section, $\sigma(\nu_\mu n \rightarrow \mu^- K^+ \Lambda^0)$. The predictions include resonant contributions only.

9. Total CC Cross Section

Figures 19-20 compare total inclusive CC cross section predictions to available experimental data. While the total cross section at high energy (DIS regime) is known to a few percent, the cross section at lower energies is much less precisely known. In particular, data measurements in the few-GeV range are generally of $\sim 10\%$ precision and come primarily from experiments which ran in the 1970's and early 1980's [31]. At these energies, it is especially challenging to model the total cross section as there are substantial overlapping contributions from QE, resonance, and DIS processes. The Monte Carlo predictions plotted in Figure 19 include all of these contributions, and are shown to agree fairly well with each other.

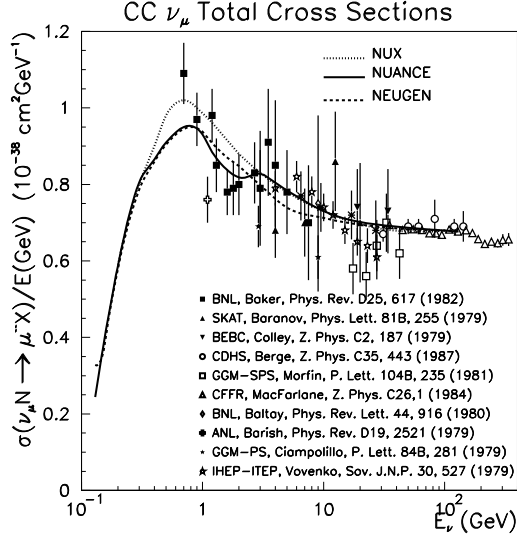


Figure 19. Total isoscalar inclusive CC cross section per GeV. The predictions are a sum of all CC contributions (i.e., QE, 1π , multi- π , DIS, etc.).

10. Conclusions

This work was an attempt to present a comprehensive comparison between available Monte Carlo generators and experimental data. While the comparisons are restricted to the case of free

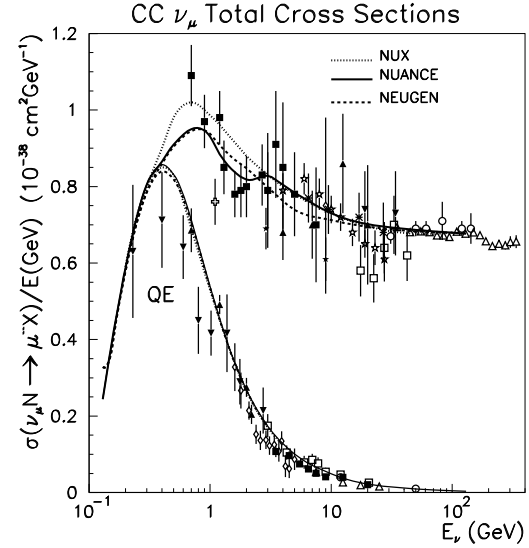


Figure 20. Same data and Monte Carlo as Figure 19 with inclusion of QE data from Figure 2.

nucleon cross sections, the hope is to expand this study to include neutrino-nucleus cross sections and predictions from additional Monte Carlo generators. In the comparisons shown here, reasonable agreement between the various Monte Carlo simulations and experimental data is observed. The agreement is slightly better for CC interactions than for NC. However, it is certainly true that the Monte Carlos agree with the experimental measurements to the extent that the data agree with themselves. Error bars in the current neutrino data set more or less span any observed differences in the Monte Carlo predictions.

11. Acknowledgments

It is a pleasure to thank D. Casper, H. Gallagher, and P. Sala for their invaluable contributions to this work and for providing their Monte Carlo predictions. In addition, the author thanks A. Bodek, J. Beacom, F. Cavanna, K. Datchev, G. Garvey, E. Hawker, and O. Palamara for useful input and discussions. Also note that data presented here will be made publicly available in the near future [32].

REFERENCES

1. P. Lipari, Nucl. Phys. Proc. Suppl. **112**, 274 (2002).
2. D. Casper, Nucl. Phys. Proc. Suppl. **112**, 161 (2002), *hep-ph/0208030*.
3. H. Gallagher, Nucl. Phys. Proc. Suppl. **112**, 188 (2002).
4. A. Rubbia, presentation at NuInt01, <http://neutrino.kek.jp/nuint01/>.
5. m_V (m_A) is determined from e^- (ν) scattering data fits, and g_A is precisely determined from neutron beta decay. The best current value for g_A is -1.267; for updated value of m_A see A. Bodek, these proceedings.
6. D. Casper, these proceedings.
7. C. H. Llewellyn Smith, Phys. Rep. **3C**, 261 (1972).
8. A. Bodek, H. Budd, J. Arrington, *hep-ex/0308005*, *hep-ex/0309024*, these proceedings.
9. L. A. Ahrens *et al.*, Phys. Rev. **D35**, 785 (1987).
10. H. Gallagher and P. Nienaber, private communication. NEUGEN assumes $\eta = +0.12$ [9] where $\Delta s \equiv g_A \eta$ implies that $\Delta s = -0.15$.
11. P. Coteus *et al.*, Phys. Rev. **D24**, 1420 (1981).
12. H. Faissner *et al.*, Phys. Rev. **D21**, 555 (1980).
13. A Entenberg *et al.*, Phys. Rev. Lett. **42**, 1198 (1979).
14. M. Pohl *et al.*, Phys. Lett. **72B**, 489 (1978).
15. F. Cavanna and O. Palamara, Nucl. Phys. Proc. Suppl. **112**, 183 (2002).
16. D. Rein and L. M. Sehgal, Annals Phys **133**, 79 (1981).
17. D. Allasia *et al.*, Nucl. Phys. **B343**, 285 (1990); A. Bodek, private communication.
18. S. J. Barish *et al.*, Phys. Rev. Lett. **33**, 448 (1974).
19. M. Derrick *et al.*, Phys. Rev. **D23**, 569 (1981).
20. E. Hawker, these proceedings.
21. G. L. Fogli and G. Nardulli, Nucl. Phys. **B165**, 162 (1980).
22. W. Krenz *et al.*, Nucl. Phys. **B135**, 45 (1978).
23. W. Lee *et al.*, Phys. Rev. Lett. **38**, 202 (1977).
24. P. Nienaber, Ph. D. thesis, Univerity of Illinois at Urbana-Champaign (1988).
25. M. Derrick *et al.*, Phys. Lett. **B92**, 363 (1980).
26. N. J. Baker *et al.*, Phys. Rev. **D23**, 2495 (1982).
27. P. Vilain *et al.*, Phys. Lett. **B313**, 267 (1993).
28. D. Rein and L. M. Sehgal, Nucl. Phys. **B223**, 29 (1983).
29. A. Bodek and U. K. Yang, *hep-ex/0308007*, these proceedings.
30. R. Shrock, Phys. Rev. **D12**, 2049 (1975); A. A. Amer, Phys. Rev. **D18**, 2290 (1978); H. K. Dewan, Phys. Rev. **D24**, 2369 (1981).
31. D. Naples, these proceedings.
32. As a joint collaboration between C. Andreopoulos, H. Gallagher, E. Hawker, M. Sakuda, G. P. Zeller, and the Durham reaction database group led by M. Whalley.